



Isothermal and non-isothermal crystallization kinetics of poly(butylene succinate) with nanoprecipitated calcium carbonate as nucleating agent

Nicolas Bosq¹ · Duangdao Aht-Ong^{1,2}

Received: 23 March 2017 / Accepted: 22 December 2017 / Published online: 8 January 2018
© Akadémiai Kiadó, Budapest, Hungary 2018

Abstract

Poly(butylene succinate) (PBS) nanocomposites filled with nanoprecipitated calcium carbonate (NPCC) were prepared via melt blending. The hybrid materials were crystallized under isothermal and non-isothermal conditions in order to understand the influence of NPCC on the crystallization behavior of PBS matrix. For both of these conditions, the nucleating effect induced by the addition of NPCC was clearly shown by differential scanning calorimetry (DSC) additionally to an increase of crystallinity. The analysis of isothermal crystallization by Avrami theory allowed to notice a variation of the crystallization mechanism in the presence of the filler and the apparition of secondary stage crystallization. The nanocomposites exhibited higher nucleation activity than the neat PBS and a faster crystallization process as indicated by the values of the half-time of crystallization. Ozawa and Mo theory applied on DSC data highlighted the variations of PBS crystallization behavior in the presence of NPCC. Finally, the crystallization ability of each material was evaluated via the theories of Takhor and Augis–Bennett. The crystallization activation energy showed a promotion of polymer chain diffusion that was correlated with the simultaneous apparition of secondary crystallization stage.

Keywords Polymers · Nanostructures · Crystallization · DSC

Introduction

In the past few years, the investigation in academic research on nanocomposites has grown with a great interest [1–4]. The attention focuses particularly on nanometer-sized fillers since for the same volume fraction, they contain a billion fold number of nanoparticles compared to the usual micrometer-sized fillers [5]. Thus, hybrid nanomaterials made from thermoplastics such as poly(lactic acid)

(PLA) [6] or poly(ether ether ketone) (PEEK) [7] have been largely described in the past few years.

Among the existing thermoplastic polymers, the poly(butylene succinate) (PBS) is a semicrystalline aliphatic polyester employed in a wide range of applications due to its high mechanical properties and processability [8]. This promising thermoplastic matrix is commercially available and displays many desirable properties such as thermal and chemical resistance. The study of neat PBS crystallization has been described before in the literature. From the DSC technique, Yasuniwa and Satou [9] investigated the crystallization and melting behavior of PBS presenting different molecular weights and evidenced the presence of double melting peaks for melt crystallized samples. Besides, Yoo et al. [10] have highlighted the presence of two kinds of morphologically different crystallites of PBS. With observing the crystallites melting behavior, the authors attributed them to the original formed crystallites that melt at lower temperature and to the recrystallized crystallites that melt at higher temperature. As the PBS appears to be a promising polymeric material at industrial scale, several types of fillers such as clay [11] or carbon

Electronic supplementary material The online version of this article (<https://doi.org/10.1007/s10973-017-6952-6>) contains supplementary material, which is available to authorized users.

✉ Duangdao Aht-Ong
duangdao.a@chula.ac.th

¹ Department of Materials Science, Faculty of Science, Chulalongkorn University, Bangkok 10330, Thailand

² Center of Excellence on Petrochemicals and Materials Technology, Chulalongkorn University, Bangkok 10330, Thailand

nanotubes [12] were used to modify its microscopic structure and so its final properties. The microscopic structure is tightly linked to the crystallization of the polymer matrix and so a careful attention has to be paid on the crystallization kinetics of polymers [13, 14].

According to this, many studies investigated the effect of a filler onto the crystallization of PBS. The work of Tan et al. [15] highlighted the promotion of PBS crystallization from the presence of surface-treated carbon nanotubes. Moreover, it appeared from the work of Bian et al. [16] that the silica induces a nucleating effect onto the crystallization of this polymer. The isothermal crystallization of neat PBS was investigated previously by Papageorgiou et al. [17], but other studies focused on the isothermal crystallization of PBS/carbon nanotubes [15] and PBS/layered double hydroxide [18] systems. Calcium carbonate is as well widely used as a filler in nanocomposites materials such as plastics or rubbers [19]. Jiang et al. [20] studied the effect of nanosized calcium carbonate on the polylactic acid (PLA) crystallization. They showed that the insertion of this filler leads to an enhancement of PLA crystallization ability. Additionally, the work of Yang et al. [21] studied the crystallization of polypropylene (PP) in the presence of calcium carbonate nanoparticles. The authors highlighted then a decrease of PP crystalline size with the introduction of this filler. However up to our knowledge, no investigations were performed on PBS crystallization kinetics in the presence of nanoprecipitated calcium carbonate (NPCC).

The NPCC displays several interesting properties such as a high specific surface area and a high interaction at the interface with the polymer, inducing thus nanometer size effects. Whereas the most used industrial synthesis method corresponds to the CO₂ bubbling into slaked lime, the present nanoparticles were elaborated by nano-precipitation method. It must be stressed here that the intrinsic properties of each type of synthesized calcium carbonate nanoparticle is strongly linked to the experimental parameters, such as the type and the concentration of additives [22]. Thus, the calcium carbonate may induce different behaviors of PBS matrix crystallization according to the experimental conditions employed for its synthesis.

Consequently, this paper proposes a new detailed study of the effect of NPCC onto PBS isothermal and non-isothermal crystallization kinetics. Several studies employ the in situ polymerization of monomers in presence of nanoparticles [23, 24]. In order to disperse uniformly the nanoparticles, some methods involve specific processes, conditions and high costs that are limited to the laboratory scale. The present work shows an interest since the NPCC is synthesized ex situ. Compared to the others synthesis methods of calcium carbonate nanoparticles, the controlled nano-precipitation process allows to obtain ultrafine

calcium carbonate with a uniform shape, size and size distribution. With considering the engineering point of view, it appears that the melt blending of preexisting nanoparticles with polymers is more efficient than other methods [21]. After the elaboration of the samples and the verification of filler dispersion by scanning electron microscopy (SEM), the crystallization at different cooling rates and the melting of PBS nanocomposites were then studied by differential scanning calorimetry (DSC). The combination of thermodynamic data such as the crystallization temperature, the crystallization half-time and the melting enthalpy was used to understand the effect of NPCC onto PBS crystallization. The correlation of these data with the results of wide angle X-ray diffraction (WAXD) analysis allowed to verify the final crystalline state of the samples. From the DSC data, the isothermal crystallization was firstly analyzed by Avrami theory [25, 26]. From the non-isothermal measurements, the nucleation activity of NPCC was evaluated using Dobrevá method [27]. The non-isothermal DSC data were also computed via the theories of Ozawa [28] and Mo [29] and consequently contributed to study the crystallization kinetics of the samples. Finally, the activation energy of crystallization was investigated by Takhor [30] and Augis–Bennett [31] theories in order to highlight the crystallization ability of each material.

Materials and methods

Preparation of the nanocomposites

The PBS employed in this study has been purchased from Mitsubishi Chemical Co., Ltd., Japan. NPCC nanoparticles produced by precipitation [32] were provided by Behn Meyer Chemical, Bangkok. The average diameter of the nanoparticles is ~ 40 nm with a narrow particles size distribution of ± 15 nm and a specific surface area > 40 m² g⁻¹. These nanoparticles present a spherical morphology and a crystalline structure according to SEM observation and WAXD analysis, respectively (Online Resource). The NPCC and PBS were first dried overnight at the temperature of ~ 60 °C. PBS nanocomposites filled with 5 (PBS/NPCC5) and 10 wt.% (PBS/NPCC10) of NPCC nanoparticles were then prepared via a twin screw extruder (ThermoPRISM DSR-28, Brabender Technologie, Duisburg, Germany). A screw speed of 20 rpm was used and the temperatures used in the extruder line to process the nanocomposites were ranged between 110 and 130 °C and above the melting temperature (T_m) of PBS previously estimated at ~ 115 °C from differential scanning calorimetry (Diamond DSC, Perkin-Elmer, Norwalk, Connecticut, USA). The extrudates obtained from the twin

screw extruder were finally cut into small pellets via a cutting-machine (LZ-80/VS, Labtech Engineering Co., Ltd., Samutprakarn, Thailand) with a wheel speed of 8 m min^{-1} and a pellet length set at 2.75 mm. Finally, the pellets were placed in a compression molding machine (LP-S-50 Labtech Engineering Co., Ltd., Samutprakarn, Thailand) to fabricate composite sheets with a thickness $< 1 \text{ mm}$. The compression molding was performed by cooling the samples from $130 \text{ }^\circ\text{C}$ to room temperature at a pressure of 4 MPa.

Experimental

The morphology of the different nanocomposites was examined by scanning electron microscope (SEM JSM 6480LV, JOEL Ltd., Tokyo, Japan) using an accelerator voltage of 20 kV. Prior to the analysis, the samples were fractured at ambient temperature in order to observe the fracture surface area. The samples were then mounted on a sample holder and coated with gold using an intensity of 20 mA.

X-ray diffraction analysis was performed using a wide angle X-ray diffractometer (Bruker AXS Diffractometer D8, Bruker, Karlsruhe, Germany). The $\text{CuK}\alpha$ radiation ($k = 0.1542 \text{ nm}$) was employed for the analysis, and the sealed tube was operated at 40 kV and 40 mA. The diffraction patterns were recorded at the values of 2θ ranging from 10° to 35° with a scanning rate of $2.4^\circ \text{ min}^{-1}$. The overall degree of the crystallinity for each sample was measured as indicated in the literature [33]:

$$X_c(\text{WAXD}) = \frac{A_c}{A_c + A_a} \times 100\% \quad (1)$$

with A_c and A_a the integral area of crystal peak and the amorphous area, respectively.

DSC runs were performed on a Diamond DSC (Perkin-Elmer, Norwalk, Connecticut, USA) equipped with two platinum-iridium furnaces containing the sample and the reference. PYRIS© software was used for data analysis. Calibrations of temperature, enthalpy, and tau lag were steadily done by using indium standard. Samples of about 7 mg were placed in 40 μL aluminum crucibles hermetically sealed. All the experiments were performed under a N_2 atmosphere (80 mL min^{-1}). For isothermal measurements, the samples were melted at $180 \text{ }^\circ\text{C}$ for 1 min in order to erase their thermal history then were quickly cooled to an isothermal crystallization temperature using a cooling rate of $40 \text{ }^\circ\text{C min}^{-1}$ and held at this temperature until crystallization has completed. The isothermal crystallization temperatures employed here are 75, 75.5, 80, 82.5, 85, 87.5, and $90 \text{ }^\circ\text{C}$. This range of crystallization temperatures was selected from a previous study on the isothermal crystallization of PBS [18]. For non-isothermal

measurements, all the samples were firstly melted at $180 \text{ }^\circ\text{C}$ for 1 min in order to erase their thermal history and were crystallized using various cooling rates at 2, 5, 10, 15, and $20 \text{ }^\circ\text{C min}^{-1}$. DSC scans were repeated in order to ensure the reproducibility and the reliability of the analysis.

An optical microscope (Olympus BH2 UMA, Lake Success, New York, USA) was used to observe the morphology of PBS spherulites after its crystallization. In order to erase the thermal history, each sample was first melted at $180 \text{ }^\circ\text{C}$ via DSC; the crystals were formed by cooling down the samples until $25 \text{ }^\circ\text{C}$ with a rate of $2 \text{ }^\circ\text{C min}^{-1}$. The uniform flat film of polymer obtained after cooling was consequently placed on the microscope glass slide prior to observation.

Theoretical approaches

Avrami theory

The Avrami theory [25, 26] can be used to study isothermal crystallization [6] and is expressed as:

$$X_t = 1 - \exp(-kt^n) \quad (2)$$

with X_t the relative crystallinity at time t , k the Avrami rate constant and n the Avrami exponent. The previous equation can be modified with using a double-logarithmic function as presented in Eq. 3.

$$\ln[-\ln(1 - X_t)] = \ln k + n \ln t \quad (3)$$

The physical meaning of n corresponds to the mechanism of nucleation and growth geometry, whereas k corresponds to the overall crystallization rate constant involving both nucleation and growth rate. The plot of $\ln(-\ln(1 - X_t))$ versus $\ln t$ allows to obtain the values of n and k that are determined, respectively, from the slope and the intercept of the obtained lines.

Nucleation activity

The evaluation of the nucleating activity (Ψ) of a foreign body in a polymer matrix is performed via the method of Dobrev and Gutzow [27]. In this theory, Ψ is defined as a parameter related to the variations of nucleation process with the addition of a filler. When the filler is extremely active for the nucleation process Ψ approaches 0; however, if the filler appears to be inert, Ψ approaches 1. In the case of homogeneous nucleation, the cooling rate β is related to T_c by the equation below:

$$\ln \beta = A - \frac{B}{2.3\Delta T_c^2} \quad (4)$$

where $\Delta T_c = T_m - T_c$. For heterogeneous nucleation the equation becomes:

$$\ln \beta = A - \frac{B^*}{2.3\Delta T_c^2} \quad (5)$$

and Ψ is expressed as:

$$\psi = \frac{B^*}{B} \quad (6)$$

The plot of $\ln(\beta)$ versus $1/\Delta T_c^2$ should result in a single straight line. A is defined as the intercept, B and B^* are the slope of the straight line for the neat polymer and the nanocomposite, respectively.

Ozawa theory

The description of non-isothermal crystallization of polymers can be performed by Ozawa's method [28]. In Ozawa's method, the relative crystallinity is expressed as a function of the cooling rate (β) via the equation:

$$1 - X_c(T) = \exp[-K(T)/\beta^m] \quad (7)$$

with $K(T)$ the Ozawa crystallization rate constant and m the Ozawa exponent. The double-logarithmic form of Eq. 7 leads to the equation:

$$\ln[-\ln(1 - X_c(T))] = \ln K(T) - m \ln \beta \quad (8)$$

According to Eq. 8, the plot of $\ln(-\ln(1 - X_c(T)))$ versus $\ln \beta$ at a given temperature is represented by a straight line when the Ozawa's method is valid. In this theory, $K(T)$ is consequently calculated as the antilogarithmic value of the intercept, and m is obtained via the negative value of the slope.

Mo theory

The method developed by Mo [29] is used to describe the non-isothermal crystallization process and corresponds to the combination of Ozawa and Avrami equations:

$$\ln Z_t + n \ln t = \ln K(T) - m \ln \beta \quad (9)$$

In the non-isothermal crystallization process, the physical variables such as the degree of crystallinity X_c , the cooling rate β , and the crystallization temperature T are involved. The cooling rate is then correlated to the crystallization time or temperature and to the morphology of crystals. The model is finally expressed from Eq. 9 as defined below:

$$\ln \beta = \ln F(T) - b \ln t \quad (10)$$

with

$$F(T) = [K(T)/Z_t]^{1/m}$$

the value of the cooling rate chosen at the unit of crystallization time when the system has a certain degree of crystallinity and b the ratio of Avrami exponent to Ozawa exponent (i.e., $b = n/m$). According to Eq. 8, the plot of $\ln \beta$ against $\ln t$ results in a straight line with an intercept corresponding to $\ln F(T)$ and a slope value corresponding to $-b$.

Activation energy of crystallization

The variation in the crystallization temperature (T_c) and onset temperature (T_{on}) with β are used for the calculation of activation energy for non-isothermal crystallization (ΔE_a), via different methods. The studies of Vyazovkin [34, 35] highlighted that Kissinger method is generally inapplicable for the evaluation of activation energy concerning the processes occurring on cooling and is also subject to number of important limitations. Two other methods were thus employed hereby.

Referring to the theory of Takhor [30], the calculation of ΔE_a is performed via the equation below:

$$\frac{d(\ln \beta)}{d(1/T_c)} = -\frac{\Delta E_a}{R} \quad (11)$$

where R is the universal gas constant.

The Augis–Bennett method [31] leads to a value of ΔE_a that is calculated by the following equation:

$$\frac{d[\ln(\beta/(T_{on} - T_c))]}{d(1/T_c)} = -\frac{\Delta E_a}{R} \quad (12)$$

The values of activation energy issued from these methods are then evaluated from the slopes ($-\Delta E_a/R$) of the plot of $\ln \beta$, and $\ln(\beta/(T_{on} - T_c))$ versus $1/T_c$.

Origin 8.5 Software was employed in order to plot WAXS spectra and DSC curves and to perform the theoretical calculation mentioned above.

Results and discussion

Morphology of PBS/calcium carbonate nanocomposites

The SEM images displayed in Fig. 1a, b allow to evaluate the dispersion of NPCC nanoparticles into the PBS matrix. The observation of PBS/NPCC5 shows that the nanoparticles are homogeneously spread into the polymer matrix. No filler aggregation or phase separation is observed. The morphology of PBS/NPCC10 also presents a filler that is

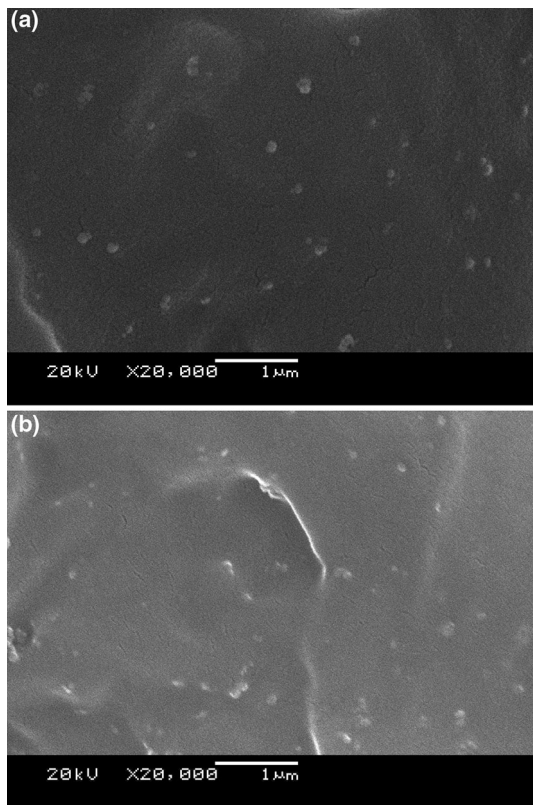


Fig. 1 SEM images of PBS filled with NPCC nanoparticles. **a** PBS/NPCC5. **b** PBS/NPCC10

homogeneously dispersed; however, some NPCC particles tend to form small clusters. This observation can be explained by the increase of NPCC amount that leads to a different arrangement of the filler into the PBS matrix.

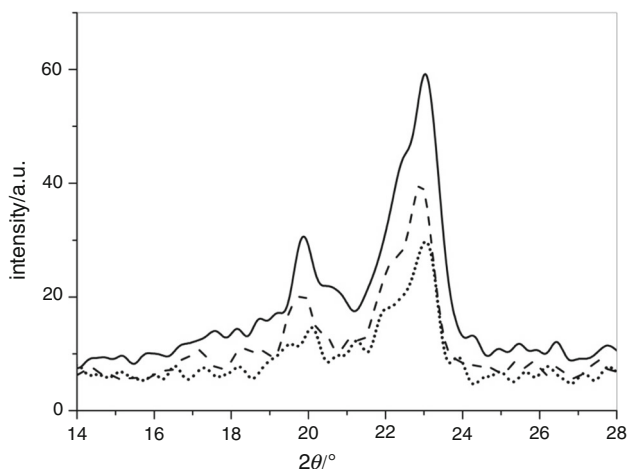


Fig. 2 WAXD patterns of (full line) neat PBS, (dash) PBS/NPCC5, (dot) PBS/NPCC10

Crystalline structure

The WAXD analysis was conducted at room temperature and the patterns are presented in Fig. 2. According to the patterns, the PBS and its nanocomposites display similar diffraction peaks. This shows that a same crystal structure is presented in the different samples and corresponds to an α -form of the PBS crystals [12]. The diffraction peaks are located at 2θ values of 19.9, 22.4, and 23.0° and are attributed, respectively, to the planes (020), (021), and (110) of the PBS crystal α -form [10]. The crystallinity from the data in Fig. 2 was found to be 42% for the neat PBS, 49% for PBS/NPCC5, and 43% for PBS/NPCC10. This result can be explained by the presence of NPCC that promotes the crystals formation and is correlated with the observation of the crystals performed by optical microscopy (OM) as presented in Online Resource. On the other hand, the crystallinity appears to be lower for PBS/NPCC10 compared to PBS/NPCC5. This result is attributed to the dispersion of the filler that is more homogeneous for the PBS filled with 5 wt.% of NPCC as observed in Fig. 1a, b.

Isothermal crystallization

Crystallization behavior

Figure 3 shows the DSC curves corresponding to the isothermal crystallization exotherms of the PBS and its nanocomposites. The thermograms clearly show that the isothermal crystallization peak of PBS filled with nanoprecipitated calcium carbonate is narrower compared to the neat PBS. This result is explained by a higher crystallization rate of PBS matrix promoted by the presence of NPCC nanoparticles. Interestingly, the nucleation effect induced by the NPCC is also highlighted in Fig. 3 by the crystallization peaks of the nanocomposites located at shorter times on the isothermal segment compared to the neat PBS. The nucleation effect that occurs during isothermal crystallization is more pronounced in the case of PBS/NPCC5 due to the more homogeneous arrangement of the filler into the polymer matrix compared to the case of PBS/NPCC10. The effect of the isothermal crystallization temperature ($T_{c(iso)}$) on the crystallization peak is obviously apparent for the neat PBS that displays a broader peak at high temperature of crystallization. The decrease of the supercooling (corresponding to the difference between the melting temperature and the crystallization temperature) consequently leads to a decrease of the crystallization rate and to an increase of the time required for the completion of crystallization. However, it is worthy to note here that crystallization peaks of PBS/NPCC nanocomposites

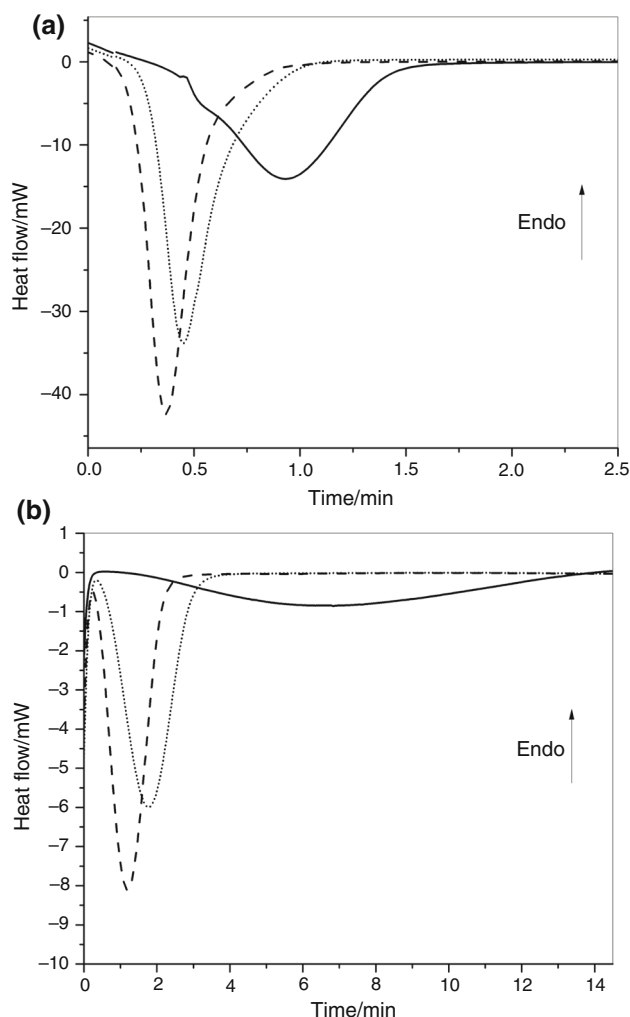


Fig. 3 DSC curves of isothermal crystallization exotherm of neat PBS (black), PBS/NPCC5 (dash), and PBS/NPCC10 (dot) for **a** $T_{c(iso)} = 75\text{ }^{\circ}\text{C}$ and **b** $T_{c(iso)} = 90\text{ }^{\circ}\text{C}$

remain narrow when higher crystallization temperatures are employed, and the influence of the supercooling on PBS crystallization is considerably less apparent. This result shows that the crystallization of PBS remains highly promoted by NPCC even for low values of supercooling.

Crystallization kinetics

The data from Fig. 3 can be used to investigate the relation between the relative crystallinity (X_t) and the time via the equation below:

$$X_c(T) = \frac{\int_{t_0}^t (dH_c/dT)dT}{\int_{t_0}^{t_{\infty}} (dH_c/dT)dT} = \frac{A_T}{A_{TOT}} \quad (13)$$

where t_0 and t_{∞} correspond to the beginning and end times of crystallization, respectively. The plots of X_t versus t for various $T_{c(iso)}$ are presented in Fig. 4. The curves display a regular S-like shape consistent with the processes of nucleation and growth of the crystals. Their slope is associated with the crystallization rate of the neat and nucleated PBS. The results confirm the faster rate of crystallization in the presence of NPCC by presenting a higher slope corresponding to higher rate changes of relative crystallization versus time [6]. The slope of crystallinity curves are normally lowered with increasing the value of $T_{c(iso)}$ and shows that the isothermal crystallization occurs slower when performed at high temperature. The values of the half crystallization time ($t_{1/2}$) that is defined as the time corresponding to a degree of crystallization of 50% can be used to estimate the rate of crystallization [36]. Indeed, a low value of $t_{1/2}$ corresponds to a high crystallization rate. The values of $t_{1/2}$ are listed in Table 1 for each isothermal crystallization temperature.

The values of $t_{1/2}$ normally increase with the increase of $T_{c(iso)}$. However, these values appear to be drastically lower in the case of the nanocomposites, especially for the isothermal crystallization temperatures close to the melting of PBS matrix. Indeed for $T_{c(iso)} = 90\text{ }^{\circ}\text{C}$, the crystallization rate of PBS/NPCC5 appears to be 5.8-fold faster compared to the neat PBS. This promotion of crystallization rate is attributed to the presence of NPCC that increases the number of nuclei and spherulitic sites into the PBS. According to Table 1, the total heat released for each crystallization temperature (ΔH_c) is not homogeneously affected by $T_{c(iso)}$ as it was observed in a previous work [17]. However, the values of ΔH_c (i.e., the degree of crystallinity determined by the value of the equilibrium melting enthalpy 210 J g^{-1}) [37] are globally higher with the insertion of NPCC that consequently increases the crystallinity of the polymer matrix. This result can be associated with the increase of the crystal thermal stability in the presence of the filler, as observed from the melting thermograms (see Online Resource). Indeed, the value of T_{m2} is globally higher for the nanocomposites and shows that the crystals melt at higher temperatures. The equilibrium melting temperature (T_m^0) was calculated from the melting thermograms according to Hoffmann–Weeks theory [17]. T_m^0 appears to be 113.5, 115.8 and 116.8 $^{\circ}\text{C}$ for the PBS, PBS/NPCC5 and PBS/NPCC10, respectively, suggesting a higher degree of crystal perfection due to the structuring effect of the filler that present a homogeneous degree of organization into the PBS matrix.

The evolution of crystallization during isothermal measurements can be understood via the Avrami theory that allows to investigate the isothermal crystallization kinetics of the different samples [25, 26]. Figure 5 displays

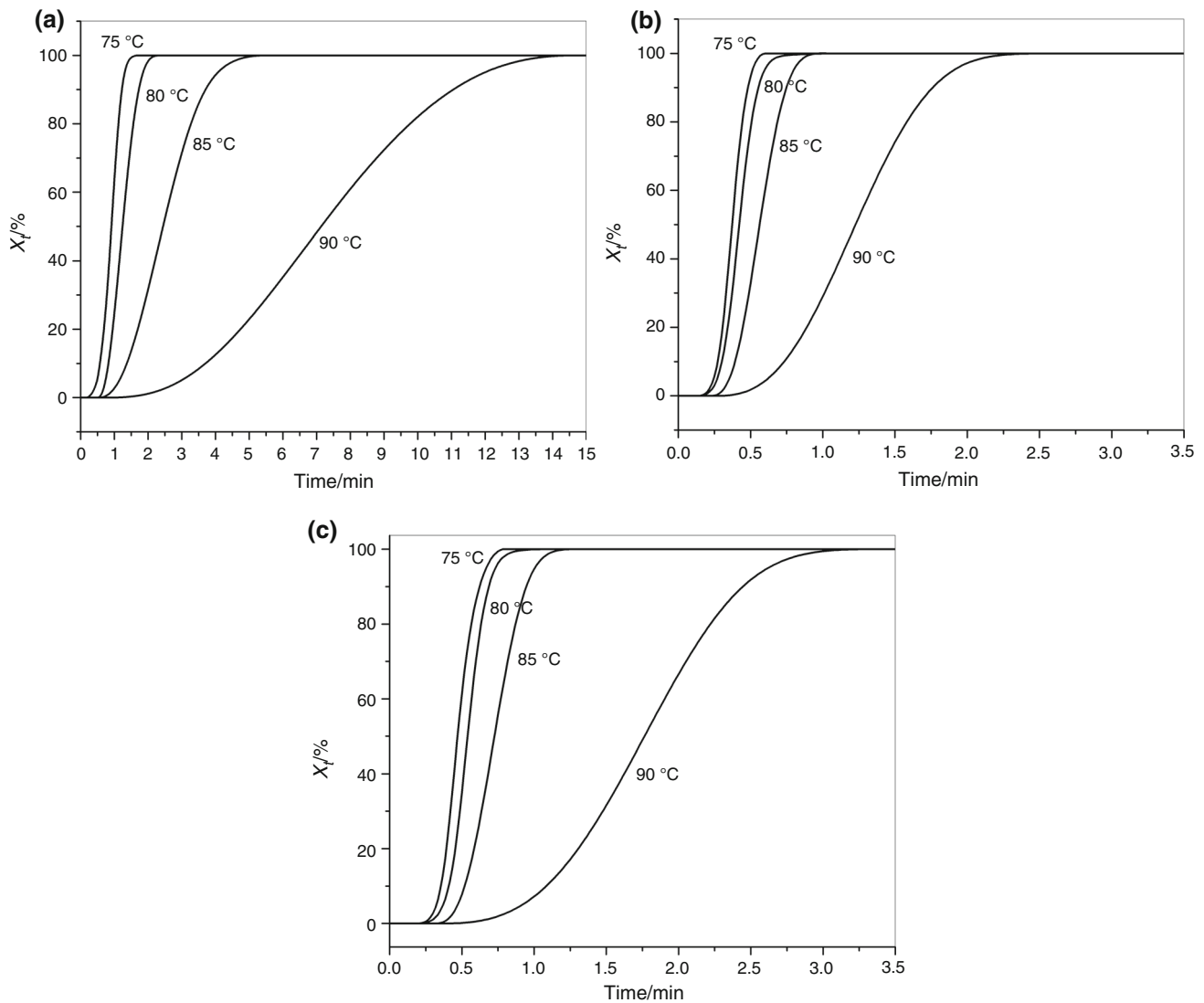


Fig. 4 Relative crystallinity (X_t) as a function of crystallization time at various crystallization temperatures for the isothermal crystallization of **a** neat PBS, **b** PBS/NPCC5, and **c** PBS/NPCC10. The value of temperature employed for isothermal crystallization is indicated by each curve

the Avrami plots for the three samples. The values of Avrami parameters n and k are listed in Table 1. The results show that the neat PBS displays a single linear region defined by a curve presenting one single slope. However, PBS/NPCC5 and PBS/NPCC10 samples display two linear regions for lower values of $T_{c(iso)}$ represented by a curve presenting two different slopes. The first linear region corresponds to the primary crystallization stage and the following leveling-off region corresponds to the secondary crystallization stage [38]. For each sample, the linear regions of the primary stage are almost parallel to each other and these linear portions are shifted toward the shorter times when $T_{c(iso)}$ decreases. The presence of these two crystallization stages for PBS/NPCC nanocomposites leads to two different values of n corresponding to n_1 and n_2 , and two values of k corresponding to k_1 and k_2 . The

deviation observed from Avrami plots and corresponding to the secondary crystallization is induced by the impingement of the spherulites occurring in the later stage of crystallization process [39]. For neat PBS, the second regime is not apparent indicating that this sample does not present any secondary crystallization process. For the lower $T_{c(iso)}$ values of PBS/NPCC nanocomposites, the Avrami curves display two linear regions and show that these samples are able to display a secondary crystallization process for specific temperatures of crystallization. The result obtained here is different from the study of Wei et al. [18] where the insertion of layered double hydroxide into the PBS does not allow to observe the secondary crystallization. This shows a new behavior of PBS crystallization mechanism with a dependence on the morphology of the filler and its arrangement into the

Table 1 Isothermal crystallization parameters of neat PBS and PBS/NPCC nanocomposites

	$T_{c(iso)}/^{\circ}\text{C}$	$t_{1/2}/\text{min}$	$\Delta H_c/\text{J g}^{-1}$	Primary stage		Secondary stage		
				n_1	k_1/min^{-n}	n_2	k_2/min^{-n}	
PBS	75	0.91	74.8	4.04	1.01	–	–	
	77.5	0.95	68.5	3.15	0.76	–	–	
	80	1.24	53.9	3.95	0.27	–	–	
	82.5	1.59	58.2	3.26	0.15	–	–	
	85	2.44	65.7	3.01	0.05	–	–	
	87.5	3.96	62.0	2.93	0.01	–	–	
	90	7.13	60.9	2.95	0.00	–	–	
	PBS/NPCC5	75	0.37	90.9	6.25	298.90	1.97	9.30
		77.5	0.46	93.0	6.26	295.89	2.13	6.04
80		0.42	83.8	6.35	86.50	–	–	
82.5		0.47	81.1	4.62	19.30	–	–	
85		0.57	80.1	4.45	8.67	–	–	
87.5		0.73	70.6	3.92	2.36	–	–	
PBS/NPCC10	75	0.46	87.6	5.68	46.52	–	–	
	77.5	0.49	90.4	5.90	45.15	3.15	9.58	
	80	0.54	74.4	5.93	24.53	3.20	8.00	
	82.5	0.63	82.8	4.96	6.69	–	–	
	85	0.73	76.6	4.75	6.69	–	–	
	87.5	1.12	72.9	3.83	0.40	–	–	
90	1.76	72.9	3.84	0.08	–	–		

polymer matrix. Indeed, the NPCC displays a spherical morphology that is different from the morphology of layered double hydroxide. According to the theory of Avrami, $n_1 \approx 4$ corresponds to a three-dimensional spherical growth. However, it appears that the values of n_1 globally increase with the insertion of NPCC. This increase shows that the interfacial interaction between the PBS and the NPCC induces a variation of PBS crystallization mechanism [15] and modifies the three-dimensional spherical growth. Interestingly, this result is different from the work of Wei et al. [18] where the insertion of layered double hydroxide does not greatly influence the mechanism of nucleation and the crystal growth morphology. It has to be noted here that the comparison between Avrami parameters (i.e., n and k) and the overall crystallization rate is difficult since n is not constant and the unit of k is expressed in min^{-n} . However, a large amount of studies has widely and successfully used Avrami theory in the case of isothermal crystallization processes [15]. The secondary crystallization of PBS/NPCC nanocomposites displays a value of $n_2 \approx 2$ and would consequently follow a one-dimensional growth process with a thermal nucleation. Then, it must be stated here that the crystallization mechanisms during the primary and secondary stages are fundamentally different. The crystal perfecting usually proceeds during the secondary stage from the initially crystallized molecules that

display imperfections and metastable state. Table 1 displays also values of k that are higher for the nanocomposite at a given crystallization temperature. This result indicates that the NPCC acts as heterogeneous nucleating agent with promoting the overall crystallization process.

Non-isothermal crystallization

Crystallization and melting behavior

Figure 6 displays the DSC thermograms at a cooling rate of $10\text{ }^{\circ}\text{C min}^{-1}$ for neat PBS and its nanocomposites, where the exothermic peaks correspond to the crystallization of the polymer matrix. The crystallization peak temperature (T_c) is noted at 73.0, 84.3, and 81.2 $^{\circ}\text{C}$ for neat PBS, PBS/NPCC5, and PBS/NPCC10, respectively. T_c of both nanocomposites are higher compared to the unfilled matrix. This result shows that the crystallization of PBS is promoted in the presence of NPCC. However, T_c of PBS/NPCC5 appears to be higher compared to PBS/NPCC10. This effect is explained by the homogeneous dispersion of NPCC into the matrix at the ratio of 5 wt.%. At the ratio of 10 wt.%, the homogeneously dispersed fraction of the filler acts as a nucleating agent, but some clustered nanoparticles lead to a slower crystallization of the molecules located around [40]. A previous study is corroborated with this

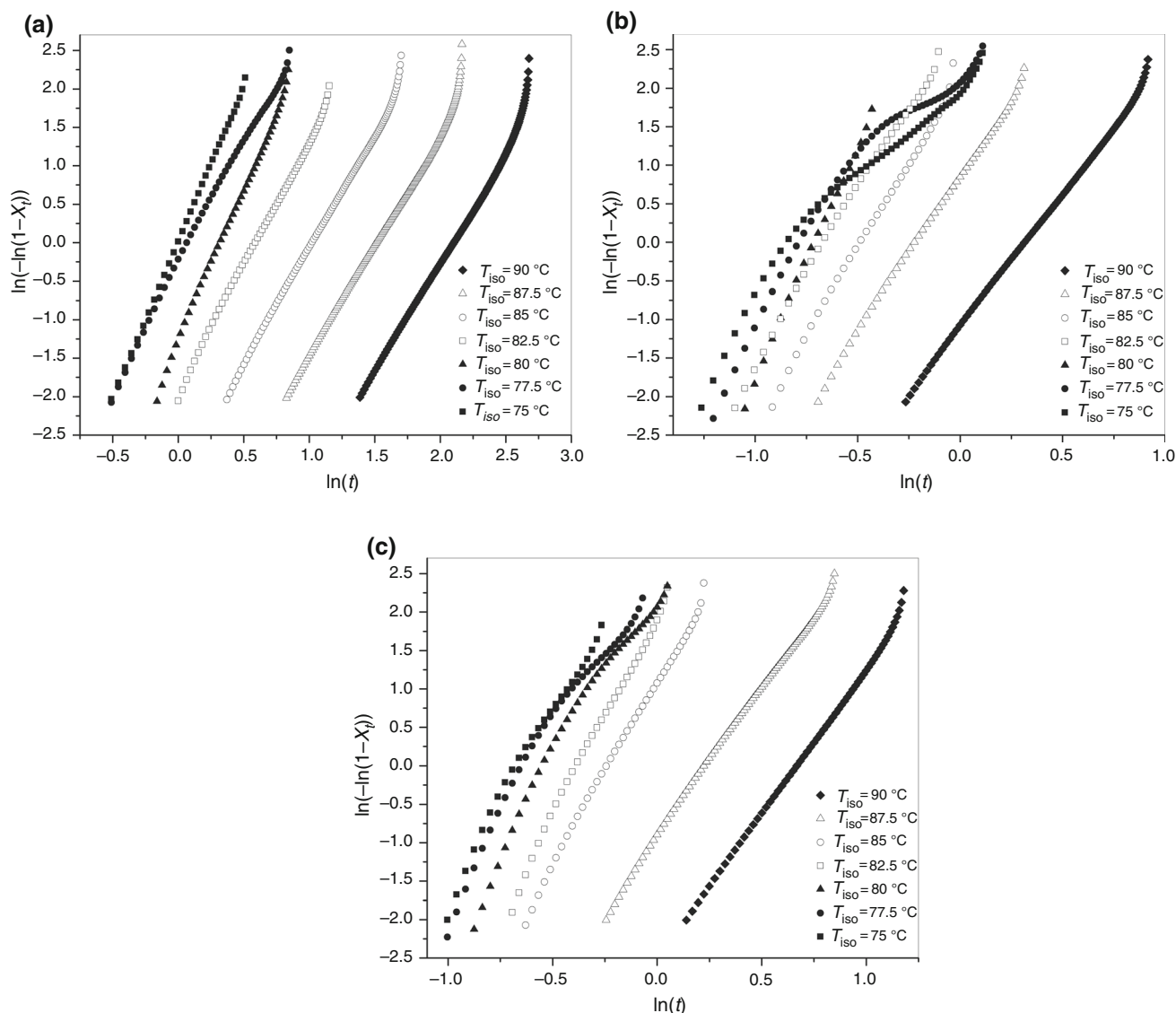


Fig. 5 Avrami plots of **a** neat PBS, **b** PBS/NPCC5, and **c** PBS/NPCC10 for isothermal crystallization at different temperatures

result by highlighting that the insertion of unmodified calcium carbonate in a polyester matrix was able to modify the crystallization process [41]. Accordingly, the present elaboration of the nanocomposite displays also an advantage since no chemistry modification of the filler surface was required to produce a nucleation effect induced by the homogeneous dispersion of NPCC into PBS. Furthermore, the crystallization peak width of PBS/NPCC5 appears to be narrower compared to the other samples and shows that the distribution of crystals formed occurs on a shorter temperature range.

The relative degree of crystallinity function with the temperature ($X_c(T)$) can be estimated from the DSC thermograms of non-isothermal crystallization scans via the following equation [42]:

$$X_c(T) = \frac{\int_{T_{on}}^T (dH_c/dT)dT}{\int_{T_{on}}^{T_{end}} (dH_c/dT)dT} = \frac{A_T}{A_{TOT}} \quad (14)$$

with T_{on} and T_{end} the temperatures at which the crystallization starts and ends, respectively, A_T the area under the crystallization peak at the temperature T , and A_{TOT} the total area of the crystallization peak. According to Eq. 14, $X_c(T)$ obtained for the three samples at a cooling rate of $10^\circ\text{C min}^{-1}$ is plotted in Fig. 7. All the crystallinity curves display a reverse sigmoidal shape. This result shows that the crystal nucleation is freely initiated from the melt state ($\sim 115^\circ\text{C}$) of the polymer. Then, the diffusion of crystal chains becomes rate determining when the temperatures are closer to the glass transition temperature

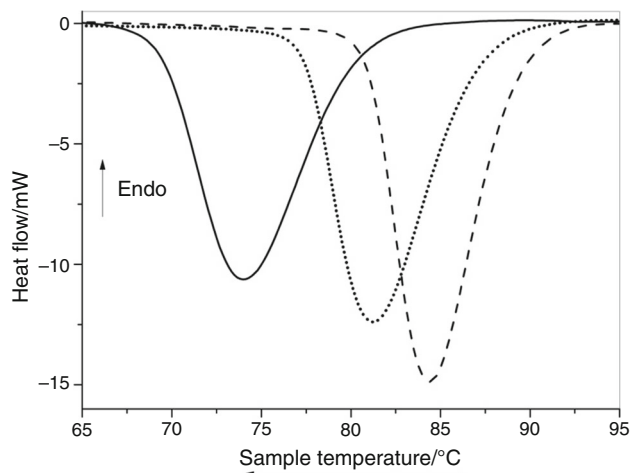


Fig. 6 DSC thermograms at the cooling rate of $10\text{ }^{\circ}\text{C min}^{-1}$. Full line: neat PBS. Dash: PBS/NPCC5. Dot: PBS/NPCC10

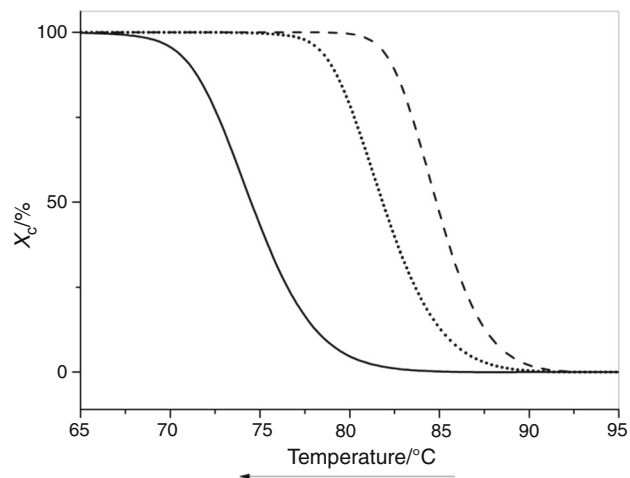


Fig. 7 X_c versus temperature for the non-isothermal crystallization at the cooling rate of $10\text{ }^{\circ}\text{C min}^{-1}$. Full line: neat PBS. Dash: PBS/NPCC5. Dot: PBS/NPCC10

($\sim -32\text{ }^{\circ}\text{C}$). As a consequence, the upper part of the plots displays a curvature that could correspond to the impingement of spherulites during the later stage of crystallization process [4]. The highest value of the onset of crystallization temperature (T_{on}) is displayed for PBS/NPCC5. This is well correlated with the results from the DSC thermograms (Fig. 6) where the most intense nucleation effect is observed for this sample. Moreover, an increase of X_c curve slope at the beginning of crystallization process is observed in the presence of NPCC, showing that the crystallization occurs faster.

Figure 8 shows the melting DSC thermograms measured on heating at $10\text{ }^{\circ}\text{C min}^{-1}$ after crystallization performed at a cooling rate of $10\text{ }^{\circ}\text{C min}^{-1}$. Two endothermic peaks can evidently be observed on the DSC thermograms. According to Yasuniwa et al. [9], the low-temperature peak

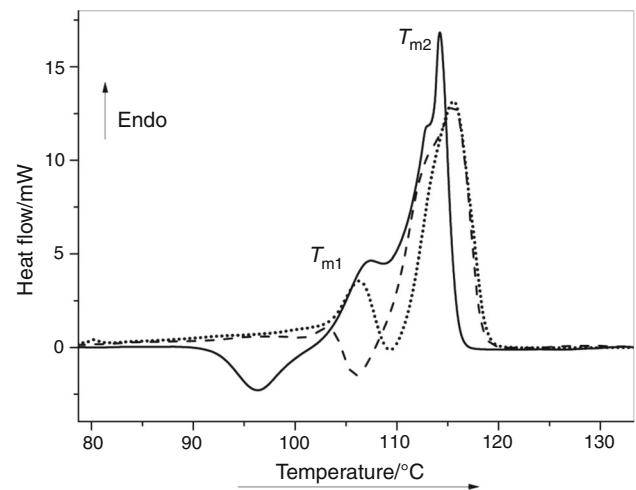


Fig. 8 Melting DSC thermograms after a cooling rate of $10\text{ }^{\circ}\text{C min}^{-1}$. Full line: neat PBS. Dash: PBS/NPCC5. Dot: PBS/NPCC10

(T_{m1}) is attributed to the melting of small and/or imperfect crystals and the high-temperature peak (T_{m2}) corresponds to the melting of more stable crystals. The crystallization process of PBS and its nanocomposites leads then to the formation of two different types of crystalline lamella [43]. It appears from the results that the value of T_{m1} is lower in presence of NPCC compared to the neat PBS. This shows that the imperfect crystals are less stable in presence of the filler. On the other hand, T_{m2} increases with the insertion of NPCC. The effect of this filler is dual since it decreases the stability of imperfect crystals and enhances simultaneously the stability of the more stable crystals. The slope of melting peak defined by T_{m2} decreases in the presence of NPCC meaning that the melting rate of the crystals formed in the nanocomposites is slower compared to neat PBS. This behavior is correlated with the increase of the crystals thermal stability in the presence of the filler. Besides, an exothermic signal is observed at $\sim 96\text{ }^{\circ}\text{C}$ on the thermogram of neat PBS. This signal was already observed in the work of Wang et al. [44] and corresponds to the re-crystallization of PBS. However, the present results show that this exothermic signal does not appear for the samples filled with NPCC implying that the insertion of filler allows to eliminate the re-crystallization process on heating.

Table 2 displays the thermodynamic parameters of each sample for crystallizations performed at various cooling rates. The value of T_{on} for each sample normally increases with the decrease of cooling rate, and the addition of NPCC into the PBS induces a global increase in T_{on} . This result shows that the introduction of the nanoparticles promotes the crystallization of PBS for all the cooling rates.

According to the data, the value of T_{m2} is not affected by the cooling rate for each sample. However, the value of T_c normally increases with decreasing the cooling rate. This

Table 2 Thermodynamic parameters of the non-isothermal crystallization of PBS and its nanocomposites

Sample	$\beta/^\circ\text{C min}^{-1}$	$T_{\text{on}}/^\circ\text{C}$	$T_c/^\circ\text{C}$	$T_{m2}/^\circ\text{C}$	$\Delta H_m/\text{J g}^{-1}$	X_c (DSC)/%	$t_{1/2}/\text{min}$
Neat PBS	20	83.4	70.4	115.0	85.3	40.6	0.63
	15	84.0	71.6	114.3	88.3	42.0	0.80
	10	85.1	73.0	114.2	90.2	43.0	1.06
	5	88.7	78.2	114.3	93.9	44.7	2.04
	2	92.5	82.7	114.2	97.3	46.3	4.70
PBS/NPCC5	20	89.2	80.2	115.6	96.7	48.5	0.45
	15	91.2	81.8	116.3	100.2	50.2	0.59
	10	93.1	84.3	115.7	103.8	52.0	0.83
	5	95.2	88.2	115.8	106.2	53.2	1.30
	2	98.8	92.4	116.3	110.2	55.2	3.05
PBS/NPCC10	20	86.3	76.2	115.5	80.5	42.6	0.49
	15	87.6	79.2	115.6	83.2	44.0	0.60
	10	90.8	81.2	115.6	88.5	46.8	0.91
	5	93.4	85.9	115.7	91.3	48.3	1.44
	2	97.2	90.6	115.8	95.7	50.6	3.17

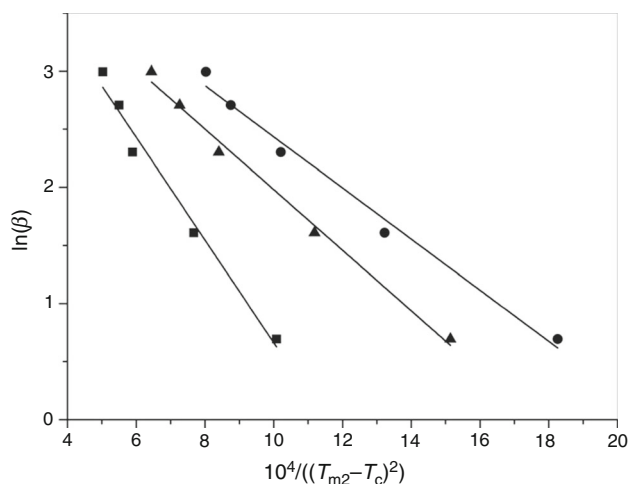
behavior is correlated with the data of the crystallization of PBS/organoclay systems [45]. An increase of T_c is observed in presence of NPCC and this increase is higher than the increment observed in the presence of cloisite organoclay [46]. For each cooling rate, it is clearly shown that PBS/NPCC5 displays the highest value of T_c . This effect is due to the homogeneous dispersion of the nanoparticles into the matrix that induces more intense nucleating effect. The degree of crystallinity (X_c) of neat PBS was calculated via the following equation:

$$X_c(\%) = \frac{\Delta H_m}{\Delta H_m^0} \times 100 \quad (15)$$

with ΔH_m the melting enthalpy of the crystalline sample, ΔH_m^0 the standard melting enthalpy of a perfect PBS crystal (210 J g^{-1}) [37]. The degree of crystallinity for PBS nanocomposites was determined by the following equation:

$$X_c(\%) = \frac{\Delta H_m}{\Delta H_m^0 \times W_f} \times 100 \quad (16)$$

with W_f the weight fraction of PBS matrix. The same standard melting enthalpy for PBS and PBS/NPCC samples is assumed here. Although a previous study highlighted a decrease of PBS crystallinity with the insertion of carbon nanotubes [12], the displayed values of X_c in Table 2 show an increase of crystallinity of PBS with the presence of NPCC. This crystallization behavior of the PBS matrix is also different from the work of Bian et al. [16] that reported similar values of X_c between the unfilled material and their silica-based nanocomposite. This behavior is due to the spherical morphology of NPCC nanoparticles. The crystallization of molecules in the polymer matrix can be sometimes hampered by the presence of the filler; however, the morphology of this latter appears not to hinder the


Fig. 9 Plots of $\ln \beta$ versus $1/\Delta T_c^2$. Squares: neat PBS. Circles: PBS/NPCC5. Triangles: PBS/NPCC10

crystallization process. In the case of NPCC, the spherical nanoparticles lead to a higher degree of crystallinity by promoting the nucleation. The crystallinity results from DSC are consistent with the data from WAXD analysis where the highest values of X_c are displayed for PBS/NPCC5 sample. The value of the half-time of crystallization ($t_{1/2}$) increases with the decrease of cooling rate for the neat PBS and its nanocomposites. Additionally, the values of $t_{1/2}$ of the nanocomposites are lower compared to the neat PBS indicating that the overall crystallization of PBS is faster in presence of the nanoparticles. Besides, the difference in $t_{1/2}$ between the neat PBS and the nanocomposites is higher at low cooling rates. The crystallization peaks obtained at low cooling rates display a T_c close to T_{m2} where the formation of stable nuclei is rate determining. The nucleating effect of NPCC is consequently

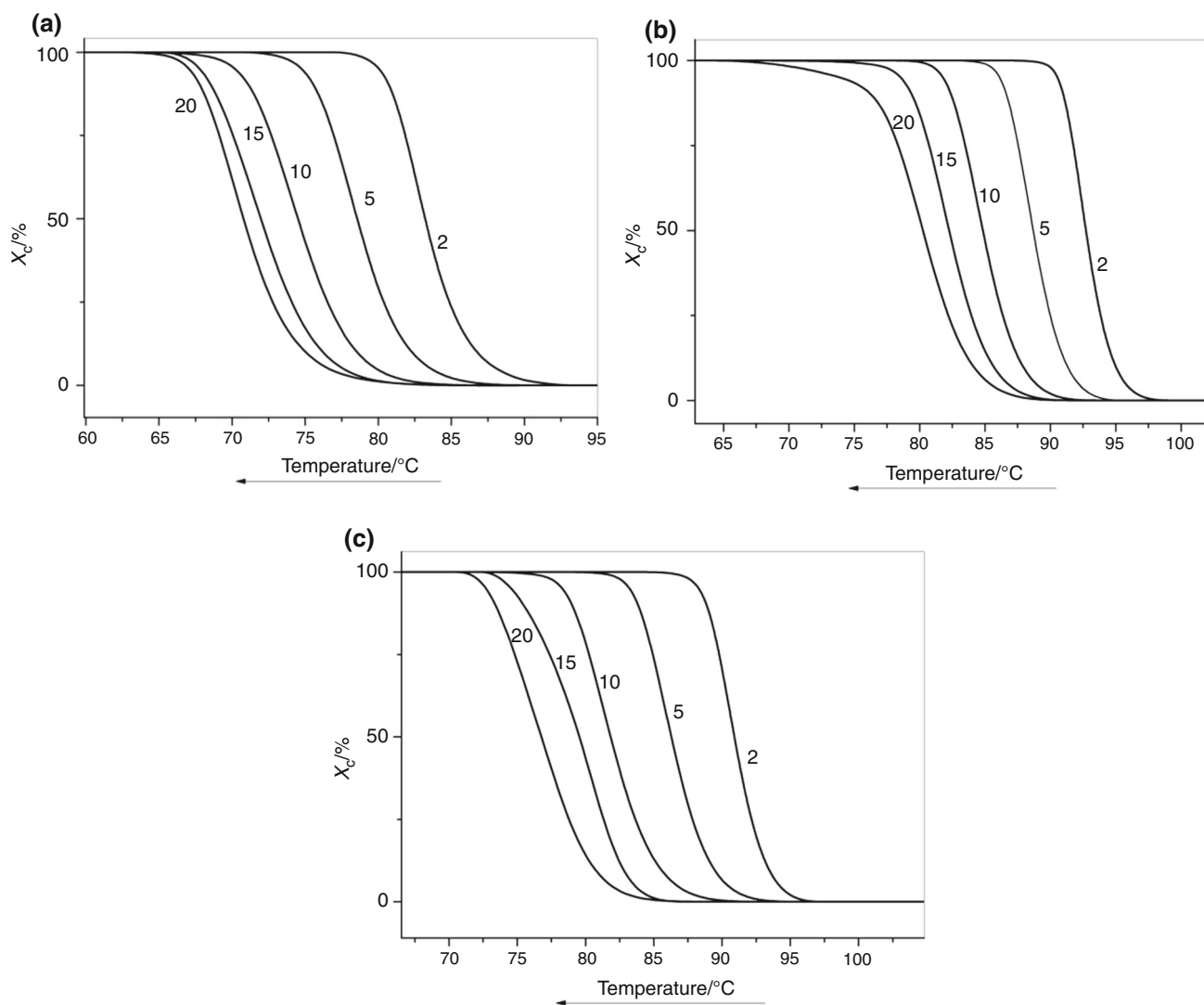


Fig. 10 X_c versus temperature at various cooling rates during the non-isothermal crystallization of **a** neat PBS, **b** PBS/NPCC5, and **c** PBS/NPCC10. The cooling rate of each experiment is indicated in $^{\circ}\text{C min}^{-1}$ by each curve

more apparent in this temperature range where the nucleation is difficult to occur and induces lower values of $t_{1/2}$ for the nanocomposites compared to the neat PBS. Conversely, for the fast cooling rates, the crystallization peaks display a T_c further from T_{m2} where the nucleation is not rate determining. The difference in $t_{1/2}$ between the neat and filled materials appears consequently to be smaller.

Nucleation activity

According to Dobreva theory [27], Fig. 9 displays the plots of $\ln \beta$ versus $1/\Delta T_c^2$ for the PBS and its nanocomposites. The value of Ψ was calculated to be 0.5 for PBS/NPCC5 and 0.6 for PBS/NPCC10. These values are lower compared to the work of Li et al. [47] who investigated the effect of clay as a nucleating agent in the polypropylene.

Thus, this result shows that the NPCC serves as an embryonic crystal or nucleus inducing the heterogeneous nucleation of polymer chains. As the NPCC nanoparticles appear to be an active substrate promoting the heterogeneous nucleation, the presence of filler consequently results in a decrease of the supercooling degree that is necessary for crystallizing nucleation.

Non-isothermal crystallization kinetics

The relative degree of crystallinity X_c at different cooling rates is presented in Fig. 10 for the neat PBS and its nanocomposites as a function of the temperature. It must be stated here that for all the cooling rates the relative extents of crystallization do not overlap each other. This important prerequisite allows to perform accurate kinetic analysis of

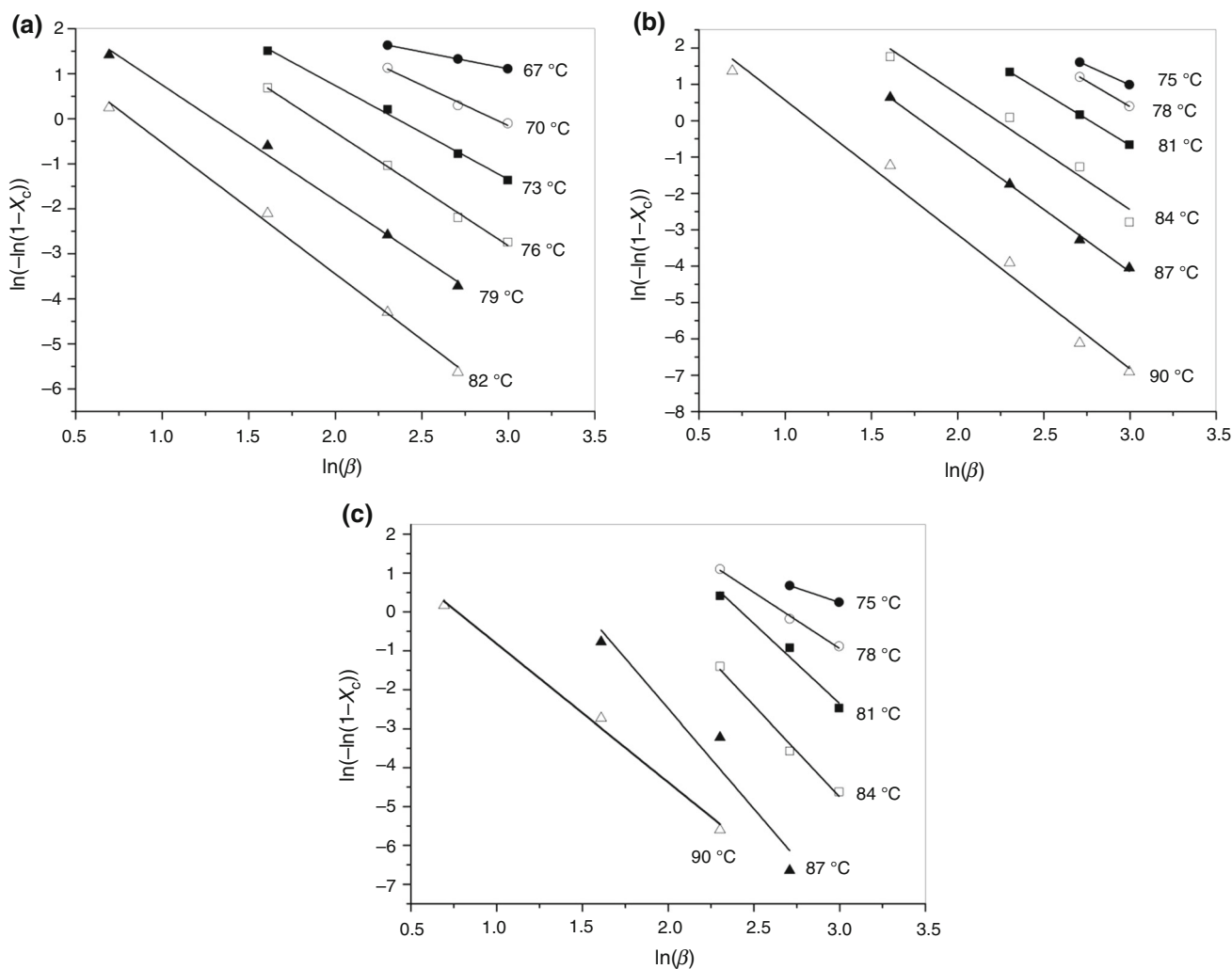


Fig. 11 Ozawa plots of $\ln(-\ln(1 - X_c))$ versus $\ln \beta$ for the non-isothermal crystallization of neat PBS (a), PBS/NPCC5 (b), PBS/NPCC10 (c)

Table 3 Non-isothermal crystallization kinetics parameters of PBS and its nanocomposites from Mo's method

Sample	Kinetic parameters	X_c /%			
		20	40	60	80
PBS	$F(T)$	8.41	10.49	12.06	13.87
	b	1.16	1.14	1.21	1.15
PBS/NPCC5	$F(T)$	5.16	6.96	8.25	9.78
	b	1.31	1.23	1.23	1.26
PBS/NPCC10	$F(T)$	6.11	7.54	9.03	11.02
	b	1.16	1.25	1.24	1.27

the crystallization. The values of X_c curves were employed for Ozawa and Mo kinetics models in order to describe the non-isothermal crystallization behavior of the different samples.

Figure 11 displays the Ozawa plots for the PBS and its nanocomposites. The investigations were carried out in the

temperature range of 67–82 °C for the neat PBS and 75–90 °C for the nanocomposites. As shown in Fig. 11, the method of Ozawa is satisfying for the description of non-isothermal crystallization of PBS and PBS/NPCC5. However, non-parallel lines are observed in the case of PBS/NPCC10. This behavior is similar to the behavior of PET and PET/clay nanocomposites from the work of Wang et al. [48]. This latter confirmed that the Ozawa approach is sometimes not able to describe the non-isothermal crystallization kinetics of polymers. However, in the present study the PBS crystallization mechanisms are different according to the quantity of filler inserted. Indeed, Ozawa approach is not valid for PBS/NPCC10 sample only, as depicted in Fig. 11c. This result can be explained by the presence of secondary stage crystallization during the non-isothermal crystallization of PBS/NPCC10 sample that is neglected in Ozawa theory [48].

The $F(T)$ and b values obtained from the application of Mo's theory [29] are presented in Table 3 and the plots are

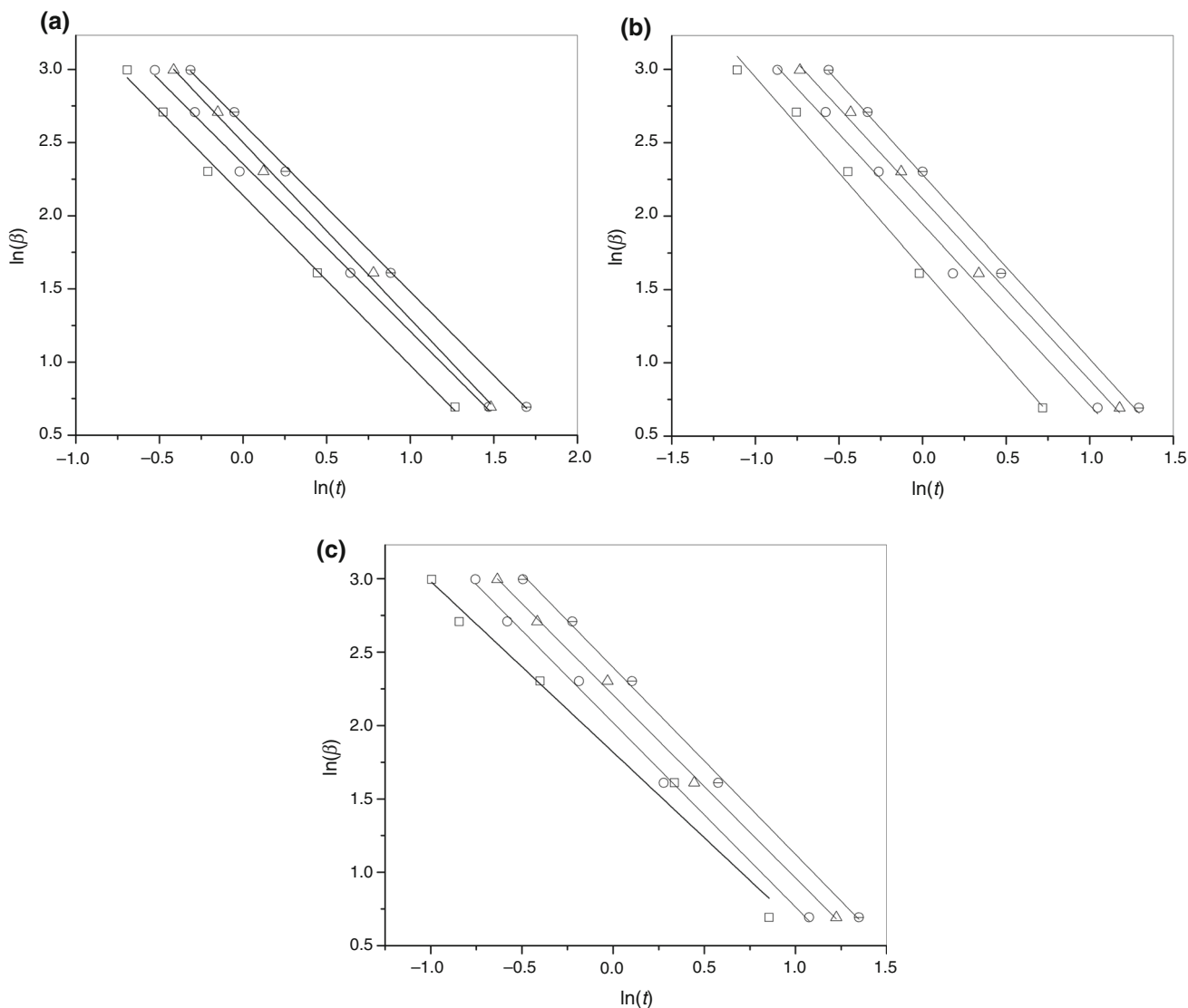


Fig. 12 Plot of $\ln \beta$ versus $\ln t$ for **a** neat PBS, **b** PBS/NPCC5 and **c** PBS/NPCC10. Squares: $X_t = 20\%$. Circles: $X_t = 40\%$. Triangles: $X_t = 60\%$. Barred circles: $X_t = 80\%$

presented in Fig. 12. Obviously, the values of $F(T)$ are lower in presence of the filler. The lowest value of $F(T)$ is observed for PBS/NPCC5. This means that to obtain a certain degree of crystallinity of the measured system, the cooling rate at the unit crystallization time that has to be employed is lower in the presence of NPCC [48]. Besides, it must be stressed out that the values of b are globally higher in presence of NPCC nanoparticles compared to the neat PBS and are correlated to a previous study about poly(oxy methylene)/montmorillonite systems [49].

Accordingly, PBS/NPCC5 sample displays a crystallization upon cooling that proceeds at higher temperature than the neat PBS and PBS/NPCC10. The behavior of the kinetic parameters $F(T)$ and b is also consistent with the results of a previous study [12] and confirms the nucleation effect induced by the filler as discussed earlier. Mo's

method consequently appears to be successful in analyzing the non-isothermal crystallization of PBS and PBS/NPCC nanocomposites, as it was highlighted from the investigations on several other systems [29, 49, 50].

Activation energy of crystallization

Figure 13 displays the plots of $\ln \beta$, and $\ln(\beta/(T_{on} - T_c))$ versus $1/T_c$ for the neat PBS and its nanocomposites. The values of ΔE_a are listed in Table 4 for each sample. The overall process of polymers crystallization combines the nucleation of crystals and the diffusion of crystals chains. In the melt state, the polymer chains are entangled, but during the crystallization these chains need to diffuse and attach onto the growing front of a crystal.

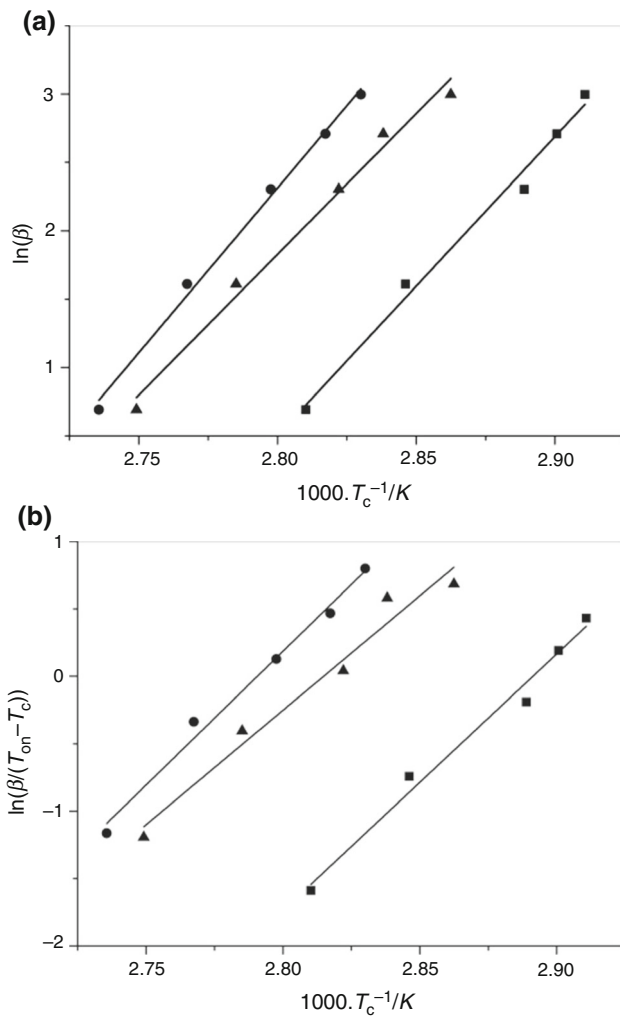


Fig. 13 Activation energy of non-isothermal crystallization from the melt via **a** Takhor and **b** Augis-Bennett methods. Squares: neat PBS. Circles: PBS/NPCC5. Triangles: PBS/NPCC10

Table 4 Values of ΔE_α for non-isothermal crystallization of PBS and its nanocomposites

Sample	$\Delta E_\alpha/kJ mol^{-1}$	
	Takhor method	Augis-Bennett method
Neat PBS	- 181	- 158
PBS/NPCC5	- 200	- 164
PBS/NPCC10	- 170	- 141

This process corresponds to a certain energy barrier that has to be overcome by the polymer chain in order to perform the crystallization. So the crystallization ability of polymers is usually related to the crystallization activation energy. The lower the crystallization ability is, the higher the activation energy is [12]. The values of ΔE_α are based

on the existing dependence of the non-isothermal crystallization peak temperature T_c on the selected cooling rates β . The amplitudes of ΔE_α variation displayed in Table 4 are larger than the amplitudes presented by Wu et al. [51], who significantly attributed them to the transport of PLA chains that is impeded in the presence of clay. The results show clearly that the absolute ΔE_α value presents the same trend for the two approaches and appears to be lower for the neat PBS compared to the PBS/NPCC5. A similar behavior of ΔE_α was already mentioned in a previous study [16] and shows that the presence of NPCC at 5 mass% induces an increase of the absolute activation energy associated with the restriction of the macromolecular segments movement. This puts in relief that the addition of NPCC at this percentage weakens the dependence of the non-isothermal crystallization peak temperatures on the employed cooling rates. The opposite behavior is observed for the PBS/NPCC10 that displays lower values of the absolute activation energy compared to the neat PBS. The transport of the macromolecular segments during the crystallization appears to be promoted with the insertion of 10 mass% of NPCC. At this percentage of NPCC, the dependence of the non-isothermal crystallization peak on the cooling rates used is strengthened. This can be due to the structuring effect of NPCC induced by the rearrangement of the filler inside the matrix. This latter may serve as a guide for the transport of the macromolecular segments and consequently promotes the crystallization ability. This effect has been highlighted in a previous study [52] where the polyethylene lamellas are intercalated between montmorillonite layers during the crystal chain expansion. Besides, this enhancement of crystallization ability is correlated with the presence of second crystallization stage for PBS/NPCC10 that is not apparent for the others samples. The insertion of 10 mass% of NPCC in the PBS matrix allows then to observe a new behavior of PBS crystallization mechanism resulting in the simultaneous polymer chain diffusion enhancement and the apparition of secondary crystallization stage. However, this promotion of the segments transport does not lead to a high increase of crystallinity. This result shows that a more efficient nucleating effect in the polymer matrix leads finally to a higher crystallinity state, compared to the case where promotion of nucleation occurs in the presence of an enhanced macromolecular segment transport.

Conclusions

The present study allowed to understand the behavior of PBS isothermal and non-isothermal crystallization behavior in presence of NPCC. PBS nanocomposites were prepared using a twin screw extruder and compression

molding machine. SEM analysis showed the homogeneous dispersion of the filler into the matrix, and the presence of small clusters in the case of PBS/NPCC10. According to WAXD analysis, the crystal structure is not influenced by the presence of NPCC. The nucleating effect induced by the presence of NPCC on the crystallization from the melt was clearly observed from the DSC thermodynamic parameters during isothermal and non-isothermal analysis. According to Avrami theory, the crystallization mechanisms of PBS are modified in the presence of NPCC and the apparition of secondary crystallization stage is promoted. The nucleation effect was confirmed by Dobreva analysis that highlighted a higher nucleation activity for the nanocomposites. Additionally, the half-time of crystallization decreased with the addition of NPCC, and the crystallinity calculated via DSC and WAXD appeared to be higher for the nanocomposites. Besides, the results of Ozawa theory were attributed to the presence of two crystallization stages for PBS/NPCC10 while Mo's theory confirmed the promotion of crystallization into the nanocomposites. The highest crystallization ability was attributed to PBS/NPCC10, due to the structuring effect induced by the arrangement of the filler in the matrix that allowed the chain transport to be more efficient during the crystallization process. The insertion of NPCC into the PBS induces consequently two different effects during the crystallization process. The calcium carbonate nanoparticles act as a heterogeneous nucleating agent by promoting the nucleation. Simultaneously, they can also conduct the crystal chain transportation by imposing surrounding constraints on the direction of crystal chain propagation with inducing additionally a secondary crystallization stage.

The great availability of PBS matrix combined with the variation of its crystallization behavior and microstructure obtained in presence of NPCC that did not require any surface modification presents then this nanocomposite as a good competitor toward the global environmental problems in various applications.

Acknowledgements The authors gratefully thank the Rachadapisek Sompot Fund for Postdoctoral Fellowship, Chulalongkorn University and the Rachadapisek Sompot Endowment under Outstanding Research Performance Program (GF-58-08-23-01) for financial support of this research.

References

- Ostovan F, Matori KA, Toozandehjani M, Oskoueian A, Yusoff HM, Yunus R, Ariff AHM, Quah HJ, Lim WF. Effects of CNTs content and milling time on mechanical behavior of MWCNT-reinforced aluminum nanocomposites. *Mater Chem Phys*. 2015;166:160–6.
- Niespodziana K, Jurczyk K, Jakubowicz J, Jurczyk M. Fabrication and properties of titanium–hydroxyapatite nanocomposites. *Mater Chem Phys*. 2010;123:160–5.
- Kampeerapappun P, Aht-ong D, Pentrakoon D, Srikulkit K. Preparation of cassava starch/montmorillonite composite film. *Carbohydr Polym*. 2007;67:155–63.
- Kuo MC, Huang JC, Chen M. Non-isothermal crystallization kinetic behavior of alumina nanoparticle filled poly(ether ether ketone). *Mater Chem Phys*. 2006;99:258–68.
- Tanaka T, Montanari GC, Mulhaupt R. Polymer nanocomposites as dielectrics and electrical insulation-perspectives for processing technologies, material characterization and future applications. *IEEE Trans Dielectr Electr Insul*. 2004;11:763–84.
- Phetwarotai W, Aht-Ong D. Isothermal crystallization behaviors and kinetics of nucleated polylactide/poly(butylene adipate-co-terephthalate) blend films with talc. *J Therm Anal Calorim*. 2016. <https://doi.org/10.1007/s1097301656692>.
- Kuo MC, Kuo JS, Yang MH, Huang JC. On the crystallization behavior of the nano-silica filled PEEK composites. *Mat Chem Phys*. 2010;123:471–80.
- Papageorgiou GZ, Bikiaris DN. Synthesis, Cocrystallization, and Enzymatic Degradation of Novel Poly(butylene-co-propylene succinate) Copolymers. *Biomacromol*. 2007;8:2437–49.
- Yasuniwa M, Satou T. Multiple melting behavior of poly(-butylene succinate). I. Thermal analysis of melt-crystallized samples. *J Polym Sci Pol Phys*. 2002;40:2411–20.
- Yoo ES, Im SS. Melting behavior of poly(butylene succinate) during heating scan by DSC. *J Polym Sci Pol Phys*. 1999;37:1357–66.
- Sinha Ray S, Okamoto K, Okamoto M. Structure–property relationship in biodegradable poly(butylene succinate)/layered silicate nanocomposites. *Macromolecules*. 2003;36:2355–67.
- Pramoda KP, Linh NTT, Zhang C, Liu T. Multiwalled carbon nanotube nucleated crystallization behavior of biodegradable poly(butylene succinate) nanocomposites. *J Appl Polym Sci*. 2009;111:2938–45.
- Sattari M, Molazemhosseini A, Naimi-Jamal M, Khavandi A. Nonisothermal crystallization behavior and mechanical properties of PEEK/SCF/nano-SiO₂ composites. *Mater Chem Phys*. 2014;147:942–53.
- Wang S, Zhang J. Non-isothermal crystallization kinetics of high density polyethylene/titanium dioxide composites via melt blending. *J Therm Anal Calorim*. 2014;115:63–71.
- Tan L, Chen Y, Zhou W, Ye S, Wei J. Novel approach toward poly(butylene succinate)/single-walled carbon nanotubes nanocomposites with interfacial-induced crystallization behaviors and mechanical strength. *Polymer*. 2011;52:3587–96.
- Bian J, Han L, Wang X, Wen X, Han C, Wang S, et al. Non-isothermal crystallization behavior and mechanical properties of poly (butylene succinate)/silica nanocomposites. *J Appl Polym Sci*. 2010;116:902–12.
- Papageorgiou GZ, Achilias DS, Bikiaris DN. Crystallization kinetics of biodegradable poly(butylene succinate) under isothermal and non-isothermal conditions. *Macromol Chem Phys*. 2007;208:1250–64.
- Wei Z, Chen G, Shi Y, Song P, Zhan M, Zhang W. Isothermal crystallization and mechanical properties of poly (butylene succinate)/layered double hydroxide nanocomposites. *J Polym Res*. 2012;19:9930.
- Tran HV, Tran LD, Vu HD, Thai H. Facile surface modification of nanoprecipitated calcium carbonate by adsorption of sodium stearate in aqueous solution. *Colloids Surf A*. 2010;366:95–103.
- Jiang L, Zhang J, Wolcott MP. Comparison of polylactide/nanosized calcium carbonate and polylactide/montmorillonite composites: reinforcing effects and toughening mechanisms. *Polymer*. 2007;48:7632–44.

21. Yang K, Yang Q, Li G, Sun Y, Feng D. Morphology and mechanical properties of polypropylene/calcium carbonate nanocomposites. *Mater Lett*. 2006;60:805–9.
22. Boyjoo Y, Pareek VK, Liu J. Synthesis of micro and nano-sized calcium carbonate particles and their applications. *J Mater Chem A*. 2014;2:14270–88.
23. Spange S, Grund S. Nanostructured organic-inorganic composite materials by twin polymerization of hybrid monomers. *Adv Mater*. 2009;21:2111–6.
24. Kawashima D, Aihara T, Kobayashi Y, Kyotani T, Tomita A. Preparation of mesoporous carbon from organic polymer/silica nanocomposite. *Chem Mater*. 2000;12:3397–401.
25. Avrami M. Kinetics of phase change. I General theory. *J Chem Phys*. 1939;7:1103–12.
26. Avrami M. Kinetics of phase change. II Transformation-time relations for random distribution of nuclei. *J Chem Phys*. 1940;8:212–24.
27. Dobrova A, Gutzow I. Activity of substrates in the catalyzed nucleation of glass-forming melts. I. Theory. *J Non-Cryst Solids*. 1993;162:1–12.
28. Ozawa T. Kinetics of non-isothermal crystallization. *Polymer*. 1971;12:150–8.
29. Liu TX, Mo ZS, Wang SE, Zhang HF. Nonisothermal melt and cold crystallization kinetics of poly(aryl ether ether ketone). *Polym Eng Sci*. 1997;37:568–75.
30. Takhor RL. Advances in nucleation and crystallization of glasses. Columbus OH: American Chemical Society; 1971.
31. Augis J, Bennett J. Calculation of the Avrami parameters for heterogeneous solid state reactions using a modification of the Kissinger method. *J Therm Anal Calorim*. 1978;13:283–92.
32. Lam TD, Hoang TV, Quang DT, Kim JS. Effect of nanosized and surface-modified precipitated calcium carbonate on properties of CaCO₃/polypropylene nanocomposites. *Mater Sci Eng, A*. 2009;501:87–93.
33. Chen S, Jin J, Zhang J. Non-isothermal crystallization behaviors of poly(4-methyl-pentene-1). *J Therm Anal Calorim*. 2011;103:229–36.
34. Vyazovkin S. Is the Kissinger equation applicable to the processes that occur on cooling? *Macromol Rapid Commun*. 2002;23:771–5.
35. Vyazovkin S, Burnham AK, Criado JM, Pérez-Maqueda LA, Popescu C, Sbirrazzuoli N. ICTAC Kinetics Committee recommendations for performing kinetic computations on thermal analysis data. *Thermochim Acta*. 2011;520:1–19.
36. Jiang X, Luo S, Sun K, Chen X. Effect of nucleating agents on crystallization kinetics of PET. *Express Polym Lett*. 2007;1:245–51.
37. Chrissafis K, Paraskevopoulos KM, Bikiaris DN. Thermal degradation mechanism of poly(ethylene succinate) and poly(butylene succinate): comparative study. *Thermochim Acta*. 2005;435:142–50.
38. Jain S, Goossens H, van Duin M, Lemstra P. Effect of in situ prepared silica nano-particles on non-isothermal crystallization of polypropylene. *Polymer*. 2005;46:8805–18.
39. Liu M, Zhao Q, Wang Y, Zhang C, Mo Z, Cao S. Melting behaviors, isothermal and non-isothermal crystallization kinetics of nylon 1212. *Polymer*. 2003;44:2537–45.
40. Wang KH, Choi MH, Koo CM, Xu M, Chung IJ, Jang MC, Choi SW, Song HH. Morphology and physical properties of poly(ethylene/silicate nanocomposite prepared by melt intercalation. *J Polym Sci B Polym Phys*. 2002;40:1454–63.
41. Phetwarotai W, Aht-Ong DD. Properties and nonisothermal crystallization behavior of nucleated polylactide biodegradable composite films. *Adv Mat Res*. 2012;488–489:671–5.
42. Kim SH, Ahn SH, Hirai T. Crystallization kinetics and nucleation activity of silica nanoparticle-filled poly(ethylene 2,6-naphthalate). *Polymer*. 2003;44:5625–34.
43. Ray SS, Bousmina M, Okamoto K. Structure and Properties of Nanocomposites Based on Poly(butylene succinate-co-adipate) and Organically Modified Montmorillonite. *Macromol Mater Eng*. 2005;290:759–68.
44. Wang Y, Chen S, Zhang S, Ma L, Shi G, Yang L. Crystallization and melting behavior of poly(butylene succinate)/silicon nitride composites: the influence of filler's phase structure. *Thermochim Acta*. 2016;627:68–76.
45. Chen G-X, Kim H-S, Yoon J-S. Synthesis and characterization of poly(butylene succinate)/epoxy group functionalized organoclay. *Polym Int*. 2007;56:1159–65.
46. Chen G-X, Yoon J-S. Nonisothermal crystallization kinetics of poly(butylene succinate) composites with a twice functionalized organoclay. *J Polym Sci B Polym Phys*. 2005;43:817–26.
47. Li J, Zhou C, Gang W. Study on nonisothermal crystallization of maleic anhydride grafted polypropylene/montmorillonite nanocomposite. *Polym Test*. 2003;22:217–23.
48. Wang Y, Shen C, Li H, Li Q, Chen J. Non-isothermal melt crystallization kinetics of poly(ethylene terephthalate)/clay nanocomposites. *J Appl Polym Sci*. 2004;91:308–14.
49. Xu W, Ge M, He P. Nonisothermal crystallization kinetics of polyoxymethylene/montmorillonite nanocomposite. *J Appl Polym Sci*. 2001;82:2281–9.
50. Qiu Z, Mo Z, Yu Y, Zhang H, Sheng S, Song C. Nonisothermal melt and cold crystallization kinetics of poly(aryl ether ketone ether ketone). *J Appl Polym Sci*. 2000;77:2865–71.
51. Wu D, Wu L, Wu L, Xu B, Zhang Y, Zhang M. Nonisothermal cold crystallization behavior and kinetics of polylactide/clay nanocomposites. *J Polym Sci B Polym Phys*. 2007;45:1100–13.
52. Xu J-T, Wang Q, Fan Z-Q. Non-isothermal crystallization kinetics of exfoliated and intercalated polyethylene/montmorillonite nanocomposites prepared by in situ polymerization. *Eur Polym J*. 2005;41:3011–7.